
WHEN ANSWERS STRAY FROM QUESTIONS: HALLUCINATION DETECTION VIA QUESTION-ANSWER ORTHOGONAL DECOMPOSITION

Siyang Yao

Shanghai Jiao Tong University
Shanghai, China

Erhu Feng

Shanghai Jiao Tong University
Shanghai, China

Yubin Xia

Shanghai Jiao Tong University
Shanghai, China

ABSTRACT

Hallucination detection in large language models (LLMs) requires balancing accuracy, efficiency, and robustness to distribution shift. Black-box consistency methods are effective but demand repeated inference; single-pass white-box probes are efficient yet treat answer representations in isolation, often degrading sharply under domain shift. We propose QAOD (**Q**uestion-**A**nswer **O**rthogonal **D**ecomposition), a single-pass framework that projects away the question-aligned direction from the answer representation to obtain a question-orthogonal component that suppresses domain-conditioned variation. To identify informative signals, QAOD further selects layers via diversity-penalized Fisher scoring and discriminative neurons via Fisher importance. To address both in-domain detection and cross-domain generalization, we design two complementary probing strategies: pairing the orthogonal component with question context yields a joint probe that maximizes in-domain discriminability, while using the orthogonal component alone preserves domain-agnostic factuality signals for robust transfer. QAOD’s joint probe achieves the best in-domain AUROC across all evaluated model-dataset pairs, while the orthogonal-only probe delivers the strongest OOD transfer, surpassing the best white-box baseline by up to 21% on BioASQ at under 2% of generation cost.

1 Introduction

Despite their remarkable progress in natural language generation and reasoning, large language models (LLMs) remain vulnerable to hallucination, the production of factually unsupported or fabricated content [Huang et al., 2025, Ji et al., 2023, Tonmoy et al., 2024, Zhang et al., 2025a]. This limitation continues to hinder the safe use of LLMs in high-stakes settings such as healthcare and legal services [Wang et al., 2024, Azamfirei et al., 2023].

A common strategy for hallucination detection is to sample multiple candidate answers and compare their consistency. Although effective, such black-box methods typically require repeated inference and therefore incur substantial computational overhead [Abdaljalil et al., 2025, Manakul et al., 2023, Farquhar et al., 2024]. This efficiency bottleneck has motivated a second line of work that aims to detect hallucinations from a single generation by probing internal states of the model [Azaria and Mitchell, 2023, Su et al., 2024, Sriraman et al., 2024]. These single-pass white-box methods are considerably faster, but many of them rely primarily on answer-side representations and may be sensitive to domain shift or to how factuality-related signals are entangled with contextual priors [Levinstein and Herrmann, 2024].

We take a third path: rather than comparing across multiple sampled outputs or probing the answer representation alone, QAOD (**Q**uestion-**A**nswer **O**rthogonal **D**ecomposition) exploits the geometric relationship between question and answer representations within a single forward pass. Through this geometric decomposition, we realize the following contributions:

- **Geometric decoupling for robust representations:** We introduce $\mathcal{H}_{V_{\perp}}$ by removing the question-aligned component from answer representations, suppressing domain variation while preserving the deviation signal. A joint variant $\mathcal{H}_{Q \oplus V_{\perp}}$ additionally incorporates question context for improved in-domain performance.

- **Fisher-based layer and neuron selection:** We propose a Fisher-discriminant criterion to identify informative layers and neurons in a single pass over training features, retaining the most discriminative signals without iterative optimization.
- **Efficient detection for in-domain and cross-domain settings:** The joint probe achieves the best in-domain AUROC on all evaluated model-dataset pairs and the orthogonal-only probe surpasses the strongest white-box baseline by up to 21% AUROC points on zero-shot BioASQ. Both operate in a single forward pass at under 2% of generation cost.

2 Related work

2.1 Black-box methods: uncertainty estimation

Hallucination detection has been studied extensively through output probabilities, repeated sampling, and semantic consistency. SelfCheckGPT [Manakul et al., 2023] detects hallucinations by sampling multiple responses and measuring their mutual consistency. Semantic entropy [Farquhar et al., 2024] addresses the limitation that surface-level token diversity can obscure meaning-level agreement: it clusters sampled responses by bidirectional entailment and computes entropy over semantic classes, while SINdex [Abdaljalil et al., 2025] extends this with cosine-similarity-based clustering and coherence-weighted entropy. Semantic Dispersion [Lin et al., 2024], Self-Prompt [Kadavath et al., 2022], direct verbalization [Lin et al., 2022], and ranked-voting self-consistency [Wang et al., 2025] offer further variants. These approaches are effective, but require multiple inference passes, incurring substantial computational overhead [Manakul et al., 2023, Chern et al., 2023, Kadavath et al., 2022].

2.2 White-box methods: internal state-based probing

White-box methods instead probe hidden states for factuality-related signals [Belinkov, 2022]. Prior work has shown that factual knowledge can appear as a linear direction in hidden space [Li et al., 2021, Marks and Tegmark, 2024, Zou et al., 2025], and that such internal signals can be exploited for probing even when the model output is hallucinated [Li et al., 2024]. Existing methods include lightweight classifiers on hidden states [Azaria and Mitchell, 2023, Su et al., 2024], layer-comparison strategies such as DoLa [Chuang et al., 2024], and other layer-wise or contrastive probes that aggregate intermediate representations across layers [Kim et al., 2025, Sriramanan et al., 2024, Chen et al., 2024a,b]. Despite these advances, white-box methods can still entangle domain-sensitive contextual signals with factuality-related signals, which may weaken OOD generalization [Levinstein and Herrmann, 2024]. A concurrent work, MHAD [Zhang et al., 2025b], also pools question and answer representations across multiple types and timesteps, but combines them via direct concatenation; this mechanical aggregation does not separate factuality-relevant deviation from question-conditioned context, which reduces its robustness under domain shift. As MHAD’s source code is unreleased and several implementation details are underspecified, we could only reproduce it from the paper description and therefore do not include it as a formal baseline; our reproduction trails QAOD on all four evaluated LLMs on zero-shot BioASQ, with an average gap of approximately 10% AUROC points. QAOD improves OOD robustness by explicitly projecting out the question-aligned component from the answer representation and probing the remaining question-orthogonal component.

3 Methodology

The hallucination detection framework QAOD consists of two branches. The offline branch identifies informative layers and neurons during training, while the online branch performs single-pass detection at test time. Figure 1 provides an overview of this offline-online pipeline.

3.1 Hidden state extraction

For question sequence S_Q and answer sequence S_A , we extract the final-token hidden states at each transformer layer l , denoted $h_Q^{(l)}, h_A^{(l)} \in \mathbb{R}^d$. In decoder-only models, causal self-attention ensures that the final token aggregates information from all preceding tokens [Vaswani et al., 2023], making it a natural read-out point; this choice is further supported by prior probing work showing its effectiveness for factuality detection [Azaria and Mitchell, 2023, Su et al., 2024, Li et al., 2024].

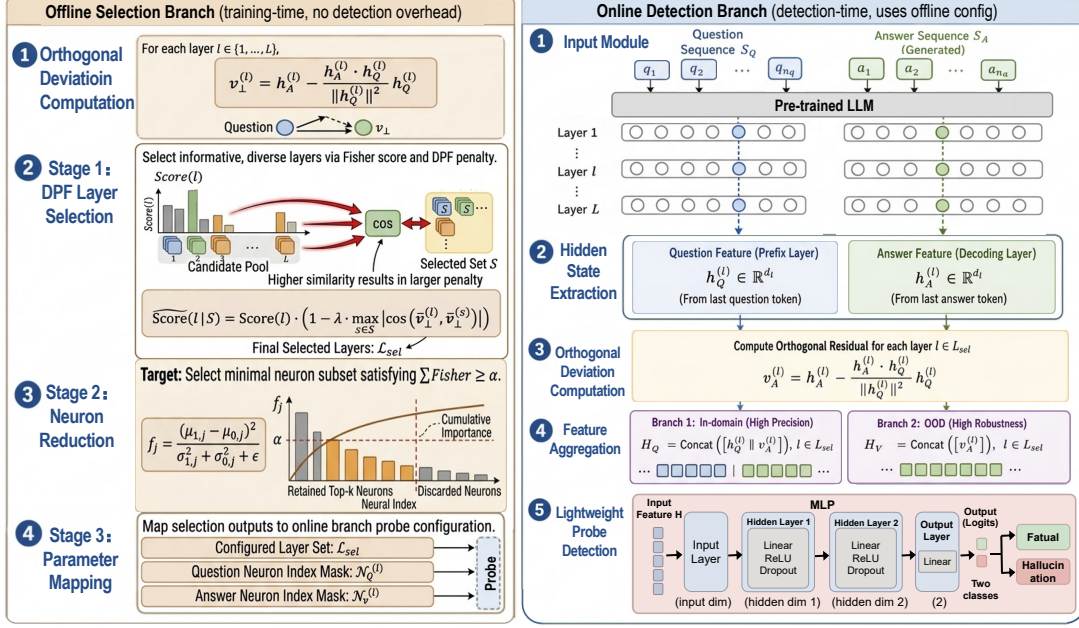


Figure 1: QAOD architecture: an offline selection branch identifies discriminative layers and neurons via Fisher-based scores; the online backbone extracts selected features and computes question-orthogonal components in a single forward pass.

3.2 Orthogonal deviation computation

For each transformer layer $l \in \{1, \dots, L\}$, we compute the question-orthogonal component $v_{\perp}^{(l)}$ by removing from the answer representation its component aligned with the question representation:

$$v_{\perp}^{(l)} = h_A^{(l)} - \text{proj}_{h_Q^{(l)}}(h_A^{(l)}) = h_A^{(l)} - \frac{h_A^{(l)} \cdot h_Q^{(l)}}{\|h_Q^{(l)}\|^2} h_Q^{(l)}. \quad (1)$$

The projection is a sample-wise decomposition step: it removes the component of $h_A^{(l)}$ collinear with the current question direction, leaving a question-orthogonal component expected to attenuate question-conditioned domain variation. Section 4.3 empirically examines whether this orthogonal decomposition improves OOD stability.

3.3 Fisher-discriminant layer and neuron selection

Given the significant depth of contemporary LLMs, naively concatenating hidden state vectors from all layers introduces severe parameter redundancy and overfitting risk. We therefore adopt a Fisher discriminant scoring procedure that operates on class-conditional statistics to identify the most informative layers and neurons for detection.

3.3.1 Layer scoring via multivariate Fisher discriminant

For each candidate layer l , we compute Fisher scores over the question representations $h_Q^{(l)}$ and the question-orthogonal components $v_{\perp}^{(l)}$. We use the score

$$F(X, y) = \frac{\|\mu_1 - \mu_0\|^2}{\text{tr}(\Sigma_1) + \text{tr}(\Sigma_0)} \quad (2)$$

where μ_c and Σ_c are the class-conditional mean and covariance estimated per label group from the training set. In our implementation, the denominator uses a per-dimension diagonal variance approximation. The layer score is $\text{Score}(l) = F(v_{\perp}^{(l)}, y)$ for $\mathcal{H}_{V_{\perp}}$, and $\text{Score}(l) = (F(h_Q^{(l)}, y) + F(v_{\perp}^{(l)}, y))/2$ for $\mathcal{H}_{Q \oplus V_{\perp}}$.

Diversity-penalized Fisher (DPF) layer selection. Pure top- K Fisher ranking tends to select consecutive layers; since adjacent layers share high inter-layer representational similarity, the resulting selection encodes largely redundant

information while missing complementary signals from distinct processing stages. We therefore employ a greedy *Diversity-Penalized Fisher* (DPF) procedure: given the set S of already-selected layers, each candidate l is scored as

$$\widetilde{\text{Score}}(l | S) = \text{Score}(l) \cdot \left(1 - \lambda \cdot \max_{s \in S} \left| \cos \left(\bar{v}_{\perp}^{(l)}, \bar{v}_{\perp}^{(s)} \right) \right| \right), \quad (3)$$

where $\bar{v}_{\perp}^{(l)}$ is the mean v_{\perp} direction at layer l and $\lambda \in [0, 1]$ controls the diversity-discriminability trade-off. At each greedy step the highest-scoring layer is added to S ; the process repeats until $|S| = K$, yielding the final selected set \mathcal{L}_{sel} .

3.3.2 Neuron selection via per-dimension Fisher scores

Within each selected layer l , we further compress representations by identifying the most discriminative neuron subsets. For each dimension $j \in \{1, \dots, d\}$, the 1D Fisher score is:

$$f_j = \frac{(\mu_{1,j} - \mu_{0,j})^2}{\sigma_{1,j}^2 + \sigma_{0,j}^2 + \epsilon}. \quad (4)$$

Neurons are ranked by f_j and selected via an α -threshold cumulative importance criterion: the smallest set of neurons whose cumulative f_j covers $\geq \alpha$ fraction of the total Fisher importance is retained. This selection is applied independently to $h_Q^{(l)}$ and $v_{\perp}^{(l)}$, respecting the geometric orthogonal decomposition and avoiding conflation of contextual priors with deviation signals. The entire selection procedure requires only a single pass over training features, accumulating class-wise statistics for closed-form ranking.

3.4 Joint feature construction

The Fisher selection procedure (Section 3.3) identifies the most discriminative neuron subsets from both h_Q and v_{\perp} . Depending on the deployment scenario, these two feature sources can be combined in different ways: incorporating h_Q provides explicit question context that can enhance in-domain discriminability, while using v_{\perp} alone yields a more domain-agnostic probe. We therefore define two probe inputs that serve these different operational priorities.

Question-orthogonal joint ($\mathcal{H}_{Q \oplus V_{\perp}}$): Concatenates question and question-orthogonal-component features, preserving both query context and deviation signal:

$$\mathcal{H}_{Q \oplus V_{\perp}} = \text{Concat} \left([h_Q^{(l)}[\mathcal{N}_Q^{(l)}], v_{\perp}^{(l)}[\mathcal{N}_v^{(l)}]] \right)_{l \in \mathcal{L}_{sel}}, \quad (5)$$

where $\mathcal{N}_Q^{(l)}$ and $\mathcal{N}_v^{(l)}$ denote the Fisher-selected neuron indices for h_Q and v_{\perp} at layer l , respectively.

Question-orthogonal component ($\mathcal{H}_{V_{\perp}}$): Uses only the question-orthogonal component:

$$\mathcal{H}_{V_{\perp}} = \text{Concat} \left(v_{\perp}^{(l)}[\mathcal{N}_v^{(l)}] \right)_{l \in \mathcal{L}_{sel}}. \quad (6)$$

The concatenated feature vector is standardized and fed into a lightweight MLP (1024 and 128 dimensions, ReLU, dropout, cross-entropy loss).

4 Experiments

4.1 Experimental setup

Benchmarks. We evaluate on four benchmarks: TriviaQA [Joshi et al., 2017], SQuAD [Rajpurkar et al., 2018], NQ (Natural Questions) [Kwiatkowski et al., 2019], and BioASQ [Krithara et al., 2022].

Models. We test on four open-weight LLMs: gemma-2-2b [Team et al., 2024], Llama-2-7B-chat [Touvron et al., 2023], Qwen3-14B [Yang et al., 2025], and Qwen3-30B-A3B [Yang et al., 2025].

Baselines. We compare against output-probability heuristics (PPL, Logit Entropy), black-box sampling consistency methods (SINDEX [Abdaljalil et al., 2025], P_{false} [Kadavath et al., 2022]), and internal state-based white-box probing methods (P_{ik} [Kadavath et al., 2022], MIND [Su et al., 2024], SAPLMA [Azaria and Mitchell, 2023], and LLM-Check [Sriramanan et al., 2024]). For SINDEX, we follow the original setting with $N = 10$ samples and `temperature=1.0`; other implementation details are provided in the appendix.

Training configuration. The QAOD probe is a two-hidden-layer MLP ($d_{in} \rightarrow 1024 \rightarrow 128 \rightarrow 2$, ReLU, dropout 0.1). Class-weighted cross-entropy is used as the loss function to handle label imbalance, with weights inversely proportional to class frequency. The model is trained for 30 epochs with Adam ($\eta = 0.001$, weight decay 0.01).

4.2 In-domain detection performance

Table 1 reports AUROC and F1 for both QAOD configurations against all baselines. Two patterns stand out:

$\mathcal{H}_{Q \oplus V_{\perp}}$ achieves the best in-domain performance, ranking first across all 16 model-dataset combinations by jointly encoding question context alongside the orthogonal deviation signal. Its advantage over the strongest single-pass baseline (SAPLMA) is consistent across all four model families, with gains of approximately 5–7 AUROC points on TriviaQA, indicating that the benefit of incorporating question context is robust to model scale and architecture. Notably, $\mathcal{H}_{Q \oplus V_{\perp}}$ consistently matches or surpasses SINDEX across all model-dataset pairs, yet requires only a single forward pass rather than ten. This suggests that internal geometric structure encodes discriminative information at least as rich as that extracted through repeated output sampling.

$\mathcal{H}_{V_{\perp}}$ remains competitive in-domain while consistently leading zero-shot OOD evaluation in Table 2. Despite using no question context, it matches or exceeds SAPLMA on three of the four models in-domain, confirming that the orthogonal decomposition alone captures strong factuality signal and making it the preferred choice when cross-domain generalization takes priority.

4.3 Cross-domain generalization

To evaluate cross-domain transferability, we train detectors on a general-domain mixture of TriviaQA, SQuAD, and NQ, and evaluate them directly on BioASQ without any target-domain fine-tuning. The BioASQ training split is used only for the in-domain results, while the zero-shot OOD setting is reserved for cross-domain evaluation.

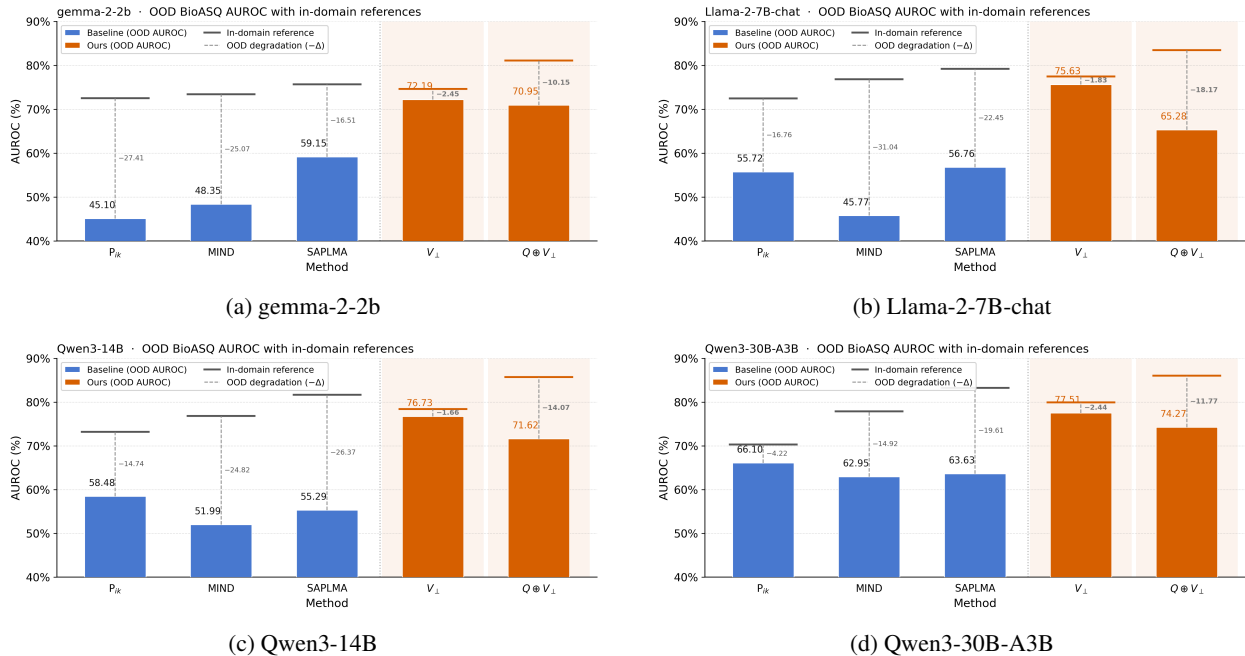


Figure 2: Zero-shot OOD AUROC on BioASQ across four LLMs. Bars show OOD AUROC for detectors trained on {TriviaQA, SQuAD, NQ} and evaluated on BioASQ; the tick marks indicate in-domain BioASQ AUROC and the dashed line the degradation gap. $\mathcal{H}_{Q \oplus V_{\perp}}$ achieves the best OOD AUROC and smallest gap.

Cross-domain generalization to BioASQ is the primary distinguishing capability of QAOD relative to existing white-box detectors. As shown in Table 2 and Figure 2, $\mathcal{H}_{V_{\perp}}$ achieves the highest zero-shot BioASQ AUROC across all four models, surpassing the strongest answer-side baseline (SAPLMA) by more than 10 AUROC points on all four models and up to 21 AUROC points, while answer-side probes degrade sharply under the source-to-target domain shift. We analyze the geometric mechanism underlying this advantage on Qwen3-14B and Qwen3-30B-A3B, which serve as representative dense and MoE backbones covering two qualitatively different architectures.

Geometric view. Figure 3 plots the normalized centroid shift $\|\mu_{\text{src}} - \mu_{\text{tgt}}\| / \bar{\sigma}$ from the source-domain mixture to BioASQ. For both representative models, the same layer-wise ordering is observed: the question-aligned component

Table 1: Hallucination detection performance on four datasets (seed=42), reporting AUROC with F1 in parentheses (%). **Bold**: best; underline: second best. QAOD_{Q⊕V⊥} ranks first on all 16 model-dataset cells.

Model	Method	TriviaQA	SQuAD	NQ	BioASQ
		AUC (F1)	AUC (F1)	AUC (F1)	AUC (F1)
gemma-2-2b	PPL	73.90 (38.28)	76.18 (40.34)	67.48 (84.22)	59.32 (69.82)
	Logit Entropy	75.59 (38.94)	77.35 (40.54)	69.14 (84.44)	64.80 (69.89)
	SINdex	80.19 (42.38)	78.26 (42.00)	75.20 (85.05)	72.91 (71.46)
	P_{false}	69.51 (35.12)	65.29 (33.65)	69.89 (83.73)	65.45 (72.34)
	LLM-Check	59.97 (27.62)	59.18 (28.13)	49.90 (83.63)	63.99 (69.14)
	P_{ik}	77.12 (41.62)	69.31 (35.16)	71.58 (83.72)	72.51 (70.35)
	MIND	76.80 (49.94)	66.76 (34.20)	72.41 (84.00)	73.42 (70.94)
	SAPLMA	<u>83.32</u> (51.42)	77.23 (42.29)	78.40 (84.96)	<u>75.66</u> (71.06)
	QAoD _{V⊥}	82.26 (52.18)	<u>79.73</u> (47.55)	77.91 (85.19)	74.64 (70.93)
	QAoD _{Q⊕V⊥}	90.10 (63.75)	82.16 (48.84)	81.42 (85.68)	81.10 (74.70)
Llama-2-7B-chat	PPL	52.16 (23.59)	56.19 (22.59)	56.81 (78.94)	53.39 (64.23)
	Logit Entropy	52.23 (23.59)	56.48 (22.59)	56.85 (78.94)	57.10 (64.23)
	SINdex	68.93 (40.65)	75.72 (39.56)	73.78 (79.72)	79.19 (68.44)
	P_{false}	65.12 (31.29)	69.42 (32.00)	68.08 (79.57)	73.76 (68.71)
	LLM-Check	65.06 (30.23)	57.35 (25.50)	56.06 (79.14)	71.40 (71.13)
	P_{ik}	75.40 (43.63)	65.93 (37.26)	62.37 (79.30)	72.48 (67.62)
	MIND	79.31 (47.32)	68.06 (36.10)	67.10 (79.72)	76.81 (72.66)
	SAPLMA	84.33 (52.74)	79.47 (43.25)	74.00 (80.90)	<u>79.21</u> (69.35)
	QAoD _{V⊥}	<u>86.20</u> (54.26)	<u>80.75</u> (44.08)	<u>75.08</u> (81.20)	77.46 (74.32)
	QAoD _{Q⊕V⊥}	90.21 (61.28)	83.09 (47.47)	77.94 (81.68)	83.45 (76.08)
Qwen3-14B	PPL	53.25 (13.13)	54.89 (14.75)	61.81 (49.47)	61.33 (46.28)
	Logit Entropy	53.25 (12.94)	54.92 (14.65)	62.06 (49.47)	61.88 (46.52)
	SINdex	65.73 (32.08)	74.02 (20.46)	78.30 (74.65)	80.50 (67.49)
	P_{false}	78.04 (32.71)	58.33 (12.33)	79.05 (77.71)	79.17 (66.97)
	LLM-Check	61.32 (21.81)	62.64 (13.06)	53.16 (77.03)	59.67 (57.42)
	P_{ik}	79.14 (39.61)	69.76 (19.45)	67.73 (70.52)	73.22 (64.13)
	MIND	81.35 (45.99)	72.12 (24.03)	73.69 (78.34)	76.81 (65.41)
	SAPLMA	85.45 (54.26)	<u>83.57</u> (29.03)	78.93 (79.03)	<u>81.66</u> (68.59)
	QAoD _{V⊥}	<u>87.42</u> (58.67)	81.34 (29.39)	79.98 (80.25)	78.39 (67.14)
	QAoD _{Q⊕V⊥}	90.13 (60.81)	85.01 (32.09)	82.69 (81.25)	85.69 (73.51)
Qwen3-30B-A3B	PPL	54.51 (16.85)	55.78 (17.74)	60.33 (77.54)	60.07 (52.34)
	Logit Entropy	54.52 (16.85)	55.82 (17.74)	60.47 (77.54)	59.73 (52.34)
	SINdex	68.26 (36.68)	74.07 (35.46)	77.33 (79.43)	81.37 (67.67)
	P_{false}	80.90 (44.52)	70.59 (22.79)	80.30 (81.84)	79.33 (66.81)
	LLM-Check	66.89 (25.95)	58.69 (18.21)	55.53 (77.52)	62.25 (55.22)
	P_{ik}	74.04 (42.11)	71.60 (27.71)	69.99 (77.61)	70.32 (59.20)
	MIND	81.38 (49.57)	72.90 (30.48)	72.69 (78.30)	77.87 (65.78)
	SAPLMA	86.74 (52.23)	<u>83.31</u> (39.76)	78.78 (80.27)	<u>83.24</u> (68.22)
	QAoD _{V⊥}	<u>87.26</u> (53.90)	82.52 (36.45)	<u>79.27</u> (80.48)	79.95 (67.85)
	QAoD _{Q⊕V⊥}	91.84 (63.89)	85.50 (40.81)	82.76 (81.76)	86.04 (73.38)

Table 2: Zero-shot cross-domain generalization to BioASQ (AUROC, %, seed=42). Detectors trained on {TriviaQA, SQuAD, NQ} are evaluated directly on BioASQ; **bold/underline**: best/second best. $\mathcal{H}_{V\perp}$ leads on all four models by a substantial margin.

Model	P_{ik}	MIND	SAPLMA	QAoD _{V⊥}	QAoD _{Q⊕V⊥}
gemma-2-2b	45.10	48.35	59.15	72.19	<u>70.95</u>
Llama-2-7B-chat	55.72	45.77	56.76	75.63	<u>65.28</u>
Qwen3-14B	58.48	51.99	55.29	76.73	<u>71.62</u>
Qwen3-30B-A3B	66.10	62.95	63.63	77.51	<u>74.27</u>

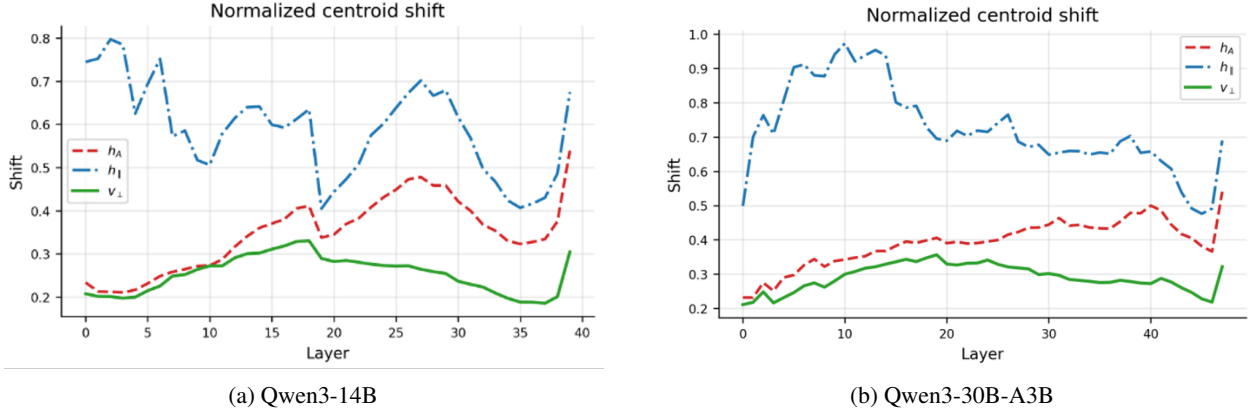


Figure 3: Layer-wise normalized centroid shift ($\|\mu_{\text{src}} - \mu_{\text{tgt}}\|/\bar{\sigma}$) from {TriviaQA, SQuAD, NQ} to BioASQ. The question-orthogonal component v_{\perp} exhibits the smallest displacement across all layers, with domain-dependent variation concentrated in the question-aligned component h_{\parallel} .

$h_{\parallel} = \frac{h_A^{(l)} \cdot h_Q^{(l)}}{\|h_Q^{(l)}\|^2} h_Q^{(l)}$ undergoes the largest displacement, the original answer state h_A lies in the middle, and the question-orthogonal component v_{\perp} is the least displaced. Much of the domain-dependent variation thus aligns with the question direction; subtracting it preserves the remaining answer information less tied to domain change.

CKA evidence. We further use linear CKA [Kornblith et al., 2019] to characterize the reduction of domain-related variation from an information-alignment perspective. Specifically, $\text{CKA}_{\text{domain}}$ measures linear alignment with domain identity ({TriviaQA, SQuAD, NQ} vs. BioASQ). Table 3 shows a consistent pattern on both Qwen3-14B and Qwen3-30B-A3B: v_{\perp} has the lowest domain alignment across all three feature-selection regimes, confirming that the question-orthogonal component suppresses domain-identity information more effectively than h_A or h_{\parallel} . The CKA result is therefore complementary to the centroid-shift analysis; the two converge on the same conclusion: v_{\perp} is less sensitive to the source-target domain change.

Importantly, CKA_{hall} for v_{\perp} is comparable to h_A in the all-layer setting and surpasses it after Fisher selection, confirming that the reduction in domain alignment does not sacrifice hallucination discriminability. The selectivity ratio $\text{CKA}_{\text{hall}}/\text{CKA}_{\text{domain}}$ captures this joint property: v_{\perp} achieves the highest ratio under every selection regime (Table 3), and Fisher selection amplifies this advantage while decreasing the ratio for h_A and h_{\parallel} , confirming that their discriminative dimensions are more entangled with domain identity.

Table 3: Linear CKA alignment with hallucination (CKA_{hall}) and domain-membership ($\text{CKA}_{\text{domain}}$) labels, and selectivity ratio, at three feature-selection operating points; v_{\perp} achieves the highest ratio under every regime, and Fisher selection widens the advantage.

Model	Selection	CKA_{hall}			$\text{CKA}_{\text{domain}}$			$\text{CKA}_{\text{hall}}/\text{CKA}_{\text{domain}}$		
		h_A	h_{\parallel}	v_{\perp}	h_A	h_{\parallel}	v_{\perp}	h_A	h_{\parallel}	v_{\perp}
Qwen3-14B	All layers	0.099	0.090	0.068	0.207	0.155	0.114	0.476	0.584	0.596
	Fisher layer	0.073	0.068	0.072	0.218	0.171	0.115	0.334	0.398	0.621
	Fisher layer+neuron	0.069	0.065	0.072	0.202	0.151	0.109	0.344	0.434	0.663
Qwen3-30B-A3B	All layers	0.083	0.077	0.080	0.269	0.226	0.149	0.310	0.343	0.537
	Fisher layer	0.059	0.046	0.076	0.240	0.196	0.137	0.244	0.237	0.556
	Fisher layer+neuron	0.056	0.044	0.077	0.236	0.184	0.136	0.239	0.238	0.564

4.4 Ablation studies

We report three ablations on Qwen3-14B and Qwen3-30B-A3B (dense and MoE representatives): a zero-shot OOD feature-construction study (trained on {TriviaQA, SQuAD, NQ}, tested on BioASQ), a layer-selection comparison on Qwen3-14B / TriviaQA, and a neuron-threshold sweep. All other settings follow the main experiments.

Feature	14B	30B
Random	64.24 ± 1.57	72.58 ± 1.66
Q-only	71.12	73.03
A-only	66.09	72.35
Q+A (no proj.)	69.88	76.11
QAOD ($\mathcal{H}_{V_{\perp}}$)	76.73	77.51

Figure 4: Feature-construction ablation: zero-shot OOD AUROC (%) on BioASQ; correct orthogonalization is necessary.

Method	$K = 5$	$K = 10$	$K = 15$	Layers ($K=5$)
Last- N layers	84.34	85.06	86.64	[35,36,37,38,39]
Pure Fisher	84.92	86.02	86.42	[19,20,21,22,23]
Uniform spacing	86.83	87.03	87.02	[0,10,20,29,39]
Random	86.49±0.43	86.74±0.19	86.86±0.37	—
DPF (ours)	87.27	87.36	87.42	[10,19,26,33,39]

Figure 5: Layer-selection ablation on Qwen3-14B / TriviaQA (AUROC, %); DPF leads at every budget and outperforms full-layer aggregation.

Table 4 holds Fisher selection fixed and varies only the feature combination. The three non-QAOD baselines all omit orthogonalization: *Random* projects the answer onto a random unit vector instead of the question direction; *Q-only* and *A-only* apply Fisher selection to h_Q or h_A alone; and *Q+A (no proj.)* follows the same Fisher selection and concatenation pipeline as QAOD but concatenates h_Q and h_A directly without computing v_{\perp} . *Random* performs worst, confirming that OOD gains require geometrically meaningful decoupling; *Q-only/A-only* each underperform QAOD, and *Q+A (no proj.)* also fails to match it, showing the advantage depends on correct question-aware orthogonalization rather than mere concatenation.

In Table 5, combining discriminability with diversity is the key factor: *Last- N layers* and pure top- K *Fisher* both select largely redundant consecutive layers, limiting coverage of complementary processing stages. *Uniform spacing* and *Random* selection improve over these by increasing layer diversity, but without discriminability guidance. DPF combines both objectives, consistently achieving the best AUROC at every budget and selecting well-spread layers (e.g., [10, 19, 26, 33, 39] for $K=5$). Using all 40 layers (AUROC 86.95) also falls below DPF at $K=15$ (87.42), confirming that diversity-aware compact selection outperforms full-depth aggregation.

Figure 6 shows performance saturating around $\alpha \in [0.8, 0.9]$; we adopt $\alpha = 0.9$ as the default.

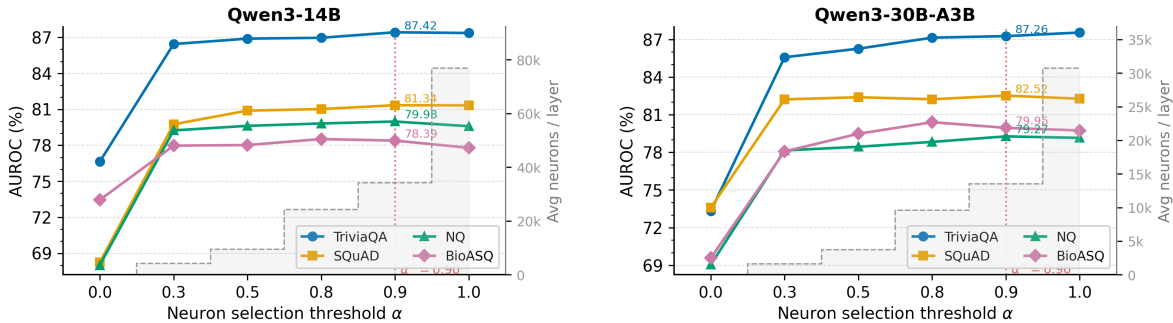


Figure 6: Neuron-selection ablation on the cumulative Fisher threshold α under $K = 15$ and $\lambda = 1$; performance stabilizes at $\alpha \in [0.8, 0.9]$, motivating the default $\alpha = 0.9$.

4.5 Efficiency

Because all methods share the same answer-generation forward pass, we compare only the additional detection overhead. Figure 7 shows the runtime breakdown on TriviaQA with Qwen3-14B (NVIDIA A100, batch size 256), highlighting the substantial computational gap between repeated-sampling methods and single-pass white-box probes in practice.

Detection overhead is orders of magnitude lower than sampling-based methods such as SINDEX ($N=10$). Among single-pass white-box probes, QAOD’s per-query detection overhead of 0.0126s is marginally higher than lighter baselines, but remains negligible relative to the shared generation cost of ~ 0.64 s ($\approx 2\%$). Given the substantial OOD robustness advantage demonstrated in Section 4.3, this marginal overhead is well-justified within the single-pass operating regime.

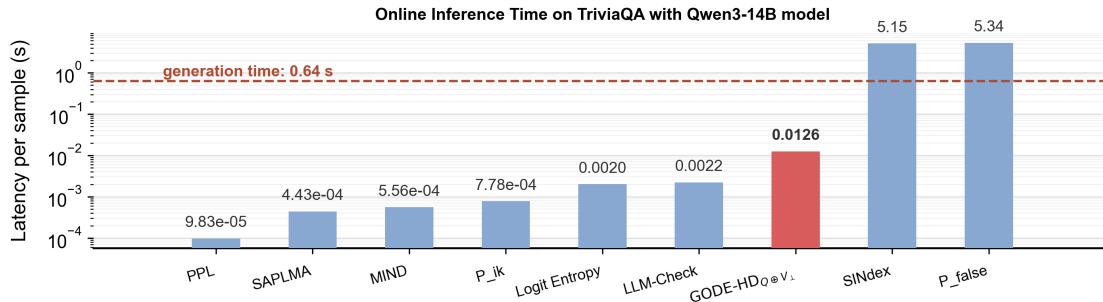


Figure 7: Inference-time comparison (log scale), including shared generation cost and additional detection overhead; QAOD’s detection cost is negligible ($\approx 2\%$) relative to generation time.

5 Limitations

The current evaluation covers knowledge-intensive QA tasks, where factual errors can often be traced to specific misapplied entities or relationships. Extending QAOD to tasks such as mathematical reasoning or open-ended generation, where the geometric properties of hidden states may differ substantially, is a promising direction for future work. Additionally, QAOD is inherently a white-box method: it requires access to intermediate hidden states of the target LLM. This makes it not directly applicable to closed-source models accessed only through inference APIs, which constitute a significant and growing fraction of deployed systems. Extending it to such settings, for instance by transferring probe knowledge from an accessible surrogate model to a black-box target, is a direction we plan to explore in future work.

6 Conclusion

In LLM hallucination detection, black-box methods demand repeated inference while white-box probes degrade sharply under domain shift. We proposed QAOD, which resolves this tension by orthogonally projecting out the question-aligned component from answer representations and applying Fisher-discriminant scoring to select compact, domain-stable probes. This is grounded in the geometric observation that domain-sensitive variation concentrates in the question-aligned direction and the residual question-orthogonal component suppresses domain-conditioned noise while retaining factuality signals. Evaluated across four LLMs and four benchmarks, $\mathcal{H}_{Q \oplus V_{\perp}}$ achieves the best in-domain AUROC on all model-dataset pairs, while $\mathcal{H}_{V_{\perp}}$ surpasses the best white-box baseline by up to 21% points on zero-shot BioASQ. These results suggest that explicitly modeling the geometric relationship between question and answer representations is a promising direction toward hallucination detectors that are simultaneously efficient and robust to domain shift, particularly in real-world settings where target-domain labels are scarce.

References

- Lei Huang, Weijiang Yu, Weitao Ma, Weihong Zhong, Zhangyin Feng, Haotian Wang, Qianglong Chen, Weihua Peng, Xiaocheng Feng, Bing Qin, and Ting Liu. A survey on hallucination in large language models: Principles, taxonomy, challenges, and open questions. *ACM Transactions on Information Systems*, 43(2):1–55, January 2025. ISSN 1558-2868. doi:10.1145/3703155. URL <http://dx.doi.org/10.1145/3703155>.
- Ziwei Ji, Nayeon Lee, Rita Frieske, Tiezheng Yu, Dan Su, Yan Xu, Etsuko Ishii, Ye Jin Bang, Andrea Madotto, and Pascale Fung. Survey of hallucination in natural language generation. *ACM Computing Surveys*, 55(12):1–38, March 2023. ISSN 1557-7341. doi:10.1145/3571730. URL <http://dx.doi.org/10.1145/3571730>.
- S. M Towhidul Islam Tonmoy, S M Mehedi Zaman, Vinija Jain, Anku Rani, Vipula Rawte, Aman Chadha, and Amitava Das. A comprehensive survey of hallucination mitigation techniques in large language models, 2024. URL <https://arxiv.org/abs/2401.01313>.
- Yue Zhang, Yafu Li, Leyang Cui, Deng Cai, Lema Liu, Tingchen Fu, Xinting Huang, Enbo Zhao, Yu Zhang, Chen Xu, Yulong Chen, Longyue Wang, Anh Tuan Luu, Wei Bi, Freda Shi, and Shuming Shi. Siren’s song in the ai ocean: A survey on hallucination in large language models, 2025a. URL <https://arxiv.org/abs/2309.01219>.
- Yuxia Wang, Minghan Wang, Muhammad Arslan Manzoor, Fei Liu, Georgi Georgiev, Rocktim Jyoti Das, and Preslav Nakov. Factuality of large language models: A survey, 2024. URL <https://arxiv.org/abs/2402.02420>.

- Razvan Azamfirei, Sapna Kudchadkar, and James Fackler. Large language models and the perils of their hallucinations. *Critical Care*, 27, 03 2023. doi:10.1186/s13054-023-04393-x.
- Samir Abdaljalil, Hasan Kurban, Parichit Sharma, Erchin Serpedin, and Rachad Atat. Sindex: Semantic inconsistency index for hallucination detection in llms, 2025. URL <https://arxiv.org/abs/2503.05980>.
- Potsawee Manakul, Adian Liusie, and Mark J. F. Gales. Selfcheckgpt: Zero-resource black-box hallucination detection for generative large language models, 2023. URL <https://arxiv.org/abs/2303.08896>.
- Sebastian Farquhar, Jannik Kossen, Lorenz Kuhn, and Yarin Gal. Detecting hallucinations in large language models using semantic entropy. *Nature*, 630(8017):625–630, 06 2024. doi:10.1038/s41586-024-07421-0. URL <https://doi.org/10.1038/s41586-024-07421-0>.
- Amos Azaria and Tom Mitchell. The internal state of an llm knows when it’s lying, 2023. URL <https://arxiv.org/abs/2304.13734>.
- Weihang Su, Changyue Wang, Qingyao Ai, Yiran Hu, Zhijing Wu, Yujia Zhou, and Yiqun Liu. Unsupervised real-time hallucination detection based on the internal states of large language models. In Lun-Wei Ku, Andre Martins, and Vivek Srikumar, editors, *Findings of the Association for Computational Linguistics: ACL 2024*, pages 14379–14391, Bangkok, Thailand, August 2024. Association for Computational Linguistics. doi:10.18653/v1/2024.findings-acl.854. URL <https://aclanthology.org/2024.findings-acl.854/>.
- Gaurang Sriramanan, Siddhant Bharti, Vinu Sankar Sadasivan, Shoumik Saha, Priyatham Kattakinda, and Soheil Feizi. Llm-check: Investigating detection of hallucinations in large language models. In A. Globerson, L. Mackey, D. Belgrave, A. Fan, U. Paquet, J. Tomczak, and C. Zhang, editors, *Advances in Neural Information Processing Systems*, volume 37, pages 34188–34216. Curran Associates, Inc., 2024. doi:10.52202/079017-1077. URL https://proceedings.neurips.cc/paper_files/paper/2024/file/3c1e1fdf305195cd620c118aaa9717ad-Paper-Conference.pdf.
- Benjamin A. Levinstein and Daniel A. Herrmann. Still no lie detector for language models: probing empirical and conceptual roadblocks. *Philosophical Studies*, 182(7):1539–1565, February 2024. ISSN 1573-0883. doi:10.1007/s11098-023-02094-3. URL <http://dx.doi.org/10.1007/s11098-023-02094-3>.
- Zhen Lin, Shubhendu Trivedi, and Jimeng Sun. Generating with confidence: Uncertainty quantification for black-box large language models, 2024. URL <https://arxiv.org/abs/2305.19187>.
- Saurav Kadavath, Tom Conerly, Amanda Askell, Tom Henighan, Dawn Drain, Ethan Perez, Nicholas Schiefer, Zac Hatfield-Dodds, Nova DasSarma, Eli Tran-Johnson, Scott Johnston, Sheer El-Showk, Andy Jones, Nelson Elhage, Tristan Hume, Anna Chen, Yuntao Bai, Sam Bowman, Stanislav Fort, Deep Ganguli, Danny Hernandez, Josh Jacobson, Jackson Kernion, Shauna Kravec, Liane Lovitt, Kamal Ndousse, Catherine Olsson, Sam Ringer, Dario Amodei, Tom Brown, Jack Clark, Nicholas Joseph, Ben Mann, Sam McCandlish, Chris Olah, and Jared Kaplan. Language models (mostly) know what they know, 2022. URL <https://arxiv.org/abs/2207.05221>.
- Stephanie Lin, Jacob Hilton, and Owain Evans. Teaching models to express their uncertainty in words, 2022. URL <https://arxiv.org/abs/2205.14334>.
- Wei Qin Wang, Yile Wang, and Hui Huang. Ranked voting based self-consistency of large language models. In Wanxiang Che, Joyce Nabende, Ekaterina Shutova, and Mohammad Taher Pilehvar, editors, *Findings of the Association for Computational Linguistics: ACL 2025*, pages 14410–14426, Vienna, Austria, July 2025. Association for Computational Linguistics. ISBN 979-8-89176-256-5. doi:10.18653/v1/2025.findings-acl.744. URL <https://aclanthology.org/2025.findings-acl.744/>.
- I-Chun Chern, Steffi Chern, Shiqi Chen, Weizhe Yuan, Kehua Feng, Chunting Zhou, Junxian He, Graham Neubig, and Pengfei Liu. Factool: Factuality detection in generative ai – a tool augmented framework for multi-task and multi-domain scenarios, 2023. URL <https://arxiv.org/abs/2307.13528>.
- Yonatan Belinkov. Probing classifiers: Promises, shortcomings, and advances. *Computational Linguistics*, 48(1): 207–219, March 2022. doi:10.1162/coli_a_00422. URL <https://aclanthology.org/2022.c1-1.7/>.
- Belinda Z. Li, Maxwell Nye, and Jacob Andreas. Implicit representations of meaning in neural language models, 2021. URL <https://arxiv.org/abs/2106.00737>.
- Samuel Marks and Max Tegmark. The geometry of truth: Emergent linear structure in large language model representations of true/false datasets, 2024. URL <https://arxiv.org/abs/2310.06824>.
- Andy Zou, Long Phan, Sarah Chen, James Campbell, Phillip Guo, Richard Ren, Alexander Pan, Xu Wang Yin, Mantas Mazeika, Ann-Kathrin Dombrowski, Shashwat Goel, Nathaniel Li, Michael J. Byun, Zifan Wang, Alex Mallen, Steven Basart, Sanmi Koyejo, Dawn Song, Matt Fredrikson, J. Zico Kolter, and Dan Hendrycks. Representation engineering: A top-down approach to ai transparency, 2025. URL <https://arxiv.org/abs/2310.01405>.

- Kenneth Li, Oam Patel, Fernanda Viégas, Hanspeter Pfister, and Martin Wattenberg. Inference-time intervention: Eliciting truthful answers from a language model, 2024. URL <https://arxiv.org/abs/2306.03341>.
- Yung-Sung Chuang, Yujia Xie, Hongyin Luo, Yoon Kim, James Glass, and Pengcheng He. Dola: Decoding by contrasting layers improves factuality in large language models, 2024. URL <https://arxiv.org/abs/2309.03883>.
- Hazel Kim, Tom A. Lamb, Adel Bibi, Philip Torr, and Yarin Gal. Detecting llm hallucination through layer-wise information deficiency: Analysis of ambiguous prompts and unanswerable questions, 2025. URL <https://arxiv.org/abs/2412.10246>.
- Yuyan Chen, Qiang Fu, Yichen Yuan, Zhihao Wen, Ge Fan, Dayiheng Liu, Dongmei Zhang, Zhixu Li, and Yanghua Xiao. Hallucination detection: Robustly discerning reliable answers in large language models, 2024a. URL <https://arxiv.org/abs/2407.04121>.
- Chao Chen, Kai Liu, Ze Chen, Yi Gu, Yue Wu, Mingyuan Tao, Zhihang Fu, and Jieping Ye. Inside: Llms’ internal states retain the power of hallucination detection, 2024b. URL <https://arxiv.org/abs/2402.03744>.
- Luan Zhang, Dandan Song, Zhijing Wu, Yuhang Tian, Changzhi Zhou, Jing Xu, Ziyi Yang, and Shuhao Zhang. Detecting hallucination in large language models through deep internal representation analysis. In James Kwok, editor, *Proceedings of the Thirty-Fourth International Joint Conference on Artificial Intelligence, IJCAI-25*, pages 8357–8365. International Joint Conferences on Artificial Intelligence Organization, 8 2025b. doi:10.24963/ijcai.2025/929. URL <https://doi.org/10.24963/ijcai.2025/929>. Main Track.
- Ashish Vaswani, Noam Shazeer, Niki Parmar, Jakob Uszkoreit, Llion Jones, Aidan N. Gomez, Lukasz Kaiser, and Illia Polosukhin. Attention is all you need, 2023. URL <https://arxiv.org/abs/1706.03762>.
- Mandar Joshi, Eunsol Choi, Daniel Weld, and Luke Zettlemoyer. TriviaQA: A large scale distantly supervised challenge dataset for reading comprehension. In Regina Barzilay and Min-Yen Kan, editors, *Proceedings of the 55th Annual Meeting of the Association for Computational Linguistics (Volume 1: Long Papers)*, pages 1601–1611, Vancouver, Canada, July 2017. Association for Computational Linguistics. doi:10.18653/v1/P17-1147. URL <https://aclanthology.org/P17-1147/>.
- Pranav Rajpurkar, Robin Jia, and Percy Liang. Know what you don’t know: Unanswerable questions for squad, 2018. URL <https://arxiv.org/abs/1806.03822>.
- Tom Kwiakowski, Jennimaria Palomaki, Olivia Redfield, Michael Collins, Ankur Parikh, Chris Alberti, Danielle Epstein, Illia Polosukhin, Jacob Devlin, Kenton Lee, Kristina Toutanova, Llion Jones, Matthew Kelcey, Ming-Wei Chang, Andrew M. Dai, Jakob Uszkoreit, Quoc Le, and Slav Petrov. Natural questions: A benchmark for question answering research. *Transactions of the Association for Computational Linguistics*, 7:453–466, 08 2019. ISSN 2307-387X. doi:10.1162/tacl_a_00276. URL https://doi.org/10.1162/tacl_a_00276.
- Anastasia Krithara, Anastasios Nentidis, Konstantinos Bougiatiotis, and Georgios Paliouras. Bioasq-qa: A manually curated corpus for biomedical question answering. *bioRxiv*, 2022. doi:10.1101/2022.12.14.520213. URL <https://www.biorxiv.org/content/early/2022/12/16/2022.12.14.520213>.
- Gemma Team, Morgane Riviere, Shreya Pathak, Pier Giuseppe Sessa, Cassidy Hardin, Surya Bhupatiraju, Léonard Hussenot, Thomas Mesnard, Bobak Shahriari, Alexandre Ramé, Johan Ferret, Peter Liu, Pouya Tafti, Abe Friesen, Michelle Casbon, Sabela Ramos, Ravin Kumar, Charline Le Lan, Sammy Jerome, Anton Tsitsulin, Nino Vieillard, Piotr Stanczyk, Sertan Girgin, Nikola Momchev, Matt Hoffman, Shantanu Thakoor, Jean-Bastien Grill, Behnam Neyshabur, Olivier Bachem, Alanna Walton, Aliaksei Severyn, Alicia Parrish, Aliya Ahmad, Allen Hutchison, Alvin Abdagic, Amanda Carl, Amy Shen, Andy Brock, Andy Coenen, Anthony Laforge, Antonia Paterson, Ben Bastian, Bilal Piot, Bo Wu, Brandon Royal, Charlie Chen, Chintu Kumar, Chris Perry, Chris Welty, Christopher A. Choquette-Choo, Danila Sinopalnikov, David Weinberger, Dimple Vijaykumar, Dominika Rogozińska, Dustin Herbison, Elisa Bandy, Emma Wang, Eric Noland, Erica Moreira, Evan Senter, Evgenii Eltyshev, Francesco Visin, Gabriel Rasskin, Gary Wei, Glenn Cameron, Gus Martins, Hadi Hashemi, Hanna Klimczak-Plucińska, Harleen Batra, Harsh Dhand, Ivan Nardini, Jacinda Mein, Jack Zhou, James Svensson, Jeff Stanway, Jetha Chan, Jin Peng Zhou, Joana Carrasqueira, Joana Iljazi, Jocelyn Becker, Joe Fernandez, Joost van Amersfoort, Josh Gordon, Josh Lipschultz, Josh Newlan, Ju yeong Ji, Kareem Mohamed, Kartikeya Badola, Kat Black, Katie Millican, Keelin McDonnell, Kelvin Nguyen, Kiranbir Sodhia, Kish Greene, Lars Lowe Sjoesund, Lauren Usui, Laurent Sifre, Lena Heuermann, Leticia Lago, Lilly McNealus, Livio Baldini Soares, Logan Kilpatrick, Lucas Dixon, Luciano Martins, Machel Reid, Manvinder Singh, Mark Iversen, Martin Görner, Mat Velloso, Mateo Wirth, Matt Davidow, Matt Miller, Matthew Rahtz, Matthew Watson, Meg Risdal, Mehran Kazemi, Michael Moynihan, Ming Zhang, Minsuk Kahng, Minwoo Park, Mofi Rahman, Mohit Khatwani, Natalie Dao, Nenshad Bardoliwalla, Nesh Devanathan, Neta Dumai, Nilay Chauhan, Oscar Wahltinez, Pankil Botarda, Parker Barnes, Paul Barham, Paul Michel, Pengchong Jin, Petko Georgiev, Phil Culliton, Pradeep Kuppala, Ramona Comanescu, Ramona Merhej, Reena Jana, Reza Ardeshtir Rokni,

Rishabh Agarwal, Ryan Mullins, Samaneh Saadat, Sara Mc Carthy, Sarah Cogan, Sarah Perrin, Sébastien M. R. Arnold, Sebastian Krause, Shengyang Dai, Shruti Garg, Shruti Sheth, Sue Ronstrom, Susan Chan, Timothy Jordan, Ting Yu, Tom Eccles, Tom Hennigan, Tomas Kocisky, Tulsee Doshi, Vihan Jain, Vikas Yadav, Vilobh Meshram, Vishal Dharmadhikari, Warren Barkley, Wei Wei, Wenming Ye, Woohyun Han, Woosuk Kwon, Xiang Xu, Zhe Shen, Zhitao Gong, Zichuan Wei, Victor Cotruta, Phoebe Kirk, Anand Rao, Minh Giang, Ludovic Peran, Tris Warkentin, Eli Collins, Joelle Barral, Zoubin Ghahramani, Raia Hadsell, D. Sculley, Jeanine Banks, Anca Dragan, Slav Petrov, Oriol Vinyals, Jeff Dean, Demis Hassabis, Koray Kavukcuoglu, Clement Farabet, Elena Buchatskaya, Sebastian Borgeaud, Noah Fiedel, Armand Joulin, Kathleen Kenealy, Robert Dadashi, and Alek Andreev. Gemma 2: Improving open language models at a practical size, 2024. URL <https://arxiv.org/abs/2408.00118>.

Hugo Touvron, Louis Martin, Kevin Stone, Peter Albert, Amjad Almahairi, Yasmine Babaei, Nikolay Bashlykov, Soumya Batra, Prajjwal Bhargava, Shruti Bhosale, Dan Bikel, Lukas Blecher, Cristian Canton Ferrer, Moya Chen, Guillem Cucurull, David Esiobu, Jude Fernandes, Jeremy Fu, Wenyin Fu, Brian Fuller, Cynthia Gao, Vedanuj Goswami, Naman Goyal, Anthony Hartshorn, Saghar Hosseini, Rui Hou, Hakan Inan, Marcin Kardas, Viktor Kerkez, Madian Khabsa, Isabel Kloumann, Artem Korenev, Punit Singh Koura, Marie-Anne Lachaux, Thibaut Lavril, Jenya Lee, Diana Liskovich, Yinghai Lu, Yuning Mao, Xavier Martinet, Todor Mihaylov, Pushkar Mishra, Igor Molybog, Yixin Nie, Andrew Poulton, Jeremy Reizenstein, Rashi Rungta, Kalyan Saladi, Alan Schelten, Ruan Silva, Eric Michael Smith, Ranjan Subramanian, Xiaoqing Ellen Tan, Binh Tang, Ross Taylor, Adina Williams, Jian Xiang Kuan, Puxin Xu, Zheng Yan, Iliyan Zarov, Yuchen Zhang, Angela Fan, Melanie Kambadur, Sharan Narang, Aurelien Rodriguez, Robert Stojnic, Sergey Edunov, and Thomas Scialom. Llama 2: Open foundation and fine-tuned chat models, 2023. URL <https://arxiv.org/abs/2307.09288>.

An Yang, Anfeng Li, Baosong Yang, Beichen Zhang, Binyuan Hui, Bo Zheng, Bowen Yu, Chang Gao, Chengen Huang, Chenxu Lv, Chujie Zheng, Dayiheng Liu, Fan Zhou, Fei Huang, Feng Hu, Hao Ge, Haoran Wei, Huan Lin, Jialong Tang, Jian Yang, Jianhong Tu, Jianwei Zhang, Jianxin Yang, Jiaxi Yang, Jing Zhou, Jingren Zhou, Junyang Lin, Kai Dang, Keqin Bao, Kexin Yang, Le Yu, Lianghao Deng, Mei Li, Mingfeng Xue, Mingze Li, Pei Zhang, Peng Wang, Qin Zhu, Rui Men, Ruize Gao, Shixuan Liu, Shuang Luo, Tianhao Li, Tianyi Tang, Wenbiao Yin, Xingzhang Ren, Xinyu Wang, Xinyu Zhang, Xuancheng Ren, Yang Fan, Yang Su, Yichang Zhang, Yinger Zhang, Yu Wan, Yuqiong Liu, Zekun Wang, Zeyu Cui, Zhenru Zhang, Zhipeng Zhou, and Zihan Qiu. Qwen3 technical report, 2025. URL <https://arxiv.org/abs/2505.09388>.

Simon Kornblith, Mohammad Norouzi, Honglak Lee, and Geoffrey Hinton. Similarity of neural network representations revisited, 2019. URL <https://arxiv.org/abs/1905.00414>.

Lianmin Zheng, Wei-Lin Chiang, Ying Sheng, Siyuan Zhuang, Zhanghao Wu, Yonghao Zhuang, Zi Lin, Zhuohan Li, Dacheng Li, Eric P. Xing, Hao Zhang, Joseph E. Gonzalez, and Ion Stoica. Judging llm-as-a-judge with mt-bench and chatbot arena, 2023. URL <https://arxiv.org/abs/2306.05685>.

A Implementation details

A.1 Label construction and judge protocol

We employed different annotation strategies depending on dataset characteristics.

SQuAD. Following the official dataset evaluation protocol, we operationalize correctness using a token-overlap F1 threshold of 50.0; answers above the threshold are treated as correct and those below it are treated as incorrect for label construction. This is a dataset-specific proxy rather than a universal hallucination definition.

TriviaQA, NQ, and BioASQ. We formulate an *LLM-as-a-judge* labeling protocol [Zheng et al., 2023] using DeepSeek-V3 as the adjudicator for semantic equivalence. When multiple reference answers are available, we ask whether the predicted answer means the same as any of the expected answers; when only one reference answer is available, we ask the same question with the singular form. In both cases, the judge is required to respond only with “yes” or “no,” following the protocol used in semantic-entropy-style semantic equivalence evaluation.

A.2 Probe configuration and optimization

For any given LLM-dataset pair, we compute multivariate Fisher scores for all layers in a single pass over training data. Unless otherwise stated, we use fixed settings across all experiments: $K = 15$ for the layer budget, $\lambda = 1$ for the diversity weight, $\alpha = 0.9$ for neuron selection, MLP hidden dimensions of 1024 and 128, Adam with learning rate $\eta = 0.001$, weight decay 0.01, and dropout probability 0.1. We adopt $\alpha = 0.9$ as a practical balance between AUROC

and feature dimensionality; this value is not claimed to be universally optimal and can be adjusted jointly with other budget choices when different deployment constraints are preferred.

Compute infrastructure. All experiments were conducted on a single NVIDIA A100 80 GB GPU. Hidden-state extraction and probe training for a given LLM-dataset pair typically complete within a few hours on this hardware; the exact wall-clock time varies with model size (e.g., shorter for Gemma-2-2B and longer for Qwen3-30B-A3B). The efficiency measurements reported in Section 4.5 were collected under the same hardware configuration with batch size 256.

A.3 Multi-seed stability on Qwen models

Table 4 summarizes the multi-seed results for Qwen3-14B and Qwen3-30B-A3B on the main in-domain benchmarks. To keep the presentation consistent with the main text, we report AUROC in percentage form here. Across both models, QAOD remains consistently the best-performing method, and the standard deviations are very small, typically below 0.4 AUROC points on TriviaQA, SQuAD, and NQ. In-domain gains are thus stable with respect to random initialization and training noise. SAPLMA, by contrast, shows a notably larger spread on BioASQ for Qwen3-14B, suggesting that some baselines are more sensitive to seed variation under domain shift.

Table 5 reports the corresponding zero-shot OOD results on BioASQ. The same pattern holds: QAOD achieves the best mean AUROC for both Qwen models, and the variance is again extremely small. Compared with the in-domain tables, the OOD setting is slightly more variable for Qwen3-14B, but the absolute standard deviations remain modest, confirming that the cross-domain advantage of the question-orthogonal component feature is not a seed artifact.

Table 4: Multi-seed in-domain AUROC on Qwen3-14B and Qwen3-30B-A3B (seeds 42 to 46, mean \pm std over five runs); QAOD achieves the lowest variance, confirming stable training.

Model	Method	TriviaQA	SQuAD	NQ	BioASQ
Qwen3-14B	MIND	82.89 \pm 0.36	72.45 \pm 1.36	74.86 \pm 1.55	78.38 \pm 1.31
	SAPLMA	86.19 \pm 0.39	83.68 \pm 0.32	79.17 \pm 0.61	78.12 \pm 4.75
	QAoD (V_{\perp})	87.25 \pm 0.24	81.39 \pm 0.37	79.62 \pm 0.21	78.15 \pm 0.08
	QAoD ($Q \oplus V_{\perp}$)	90.35 \pm 0.15	85.51 \pm 0.19	82.53 \pm 0.18	85.51 \pm 0.07
Qwen3-30B-A3B	MIND	80.38 \pm 0.61	71.88 \pm 1.00	75.39 \pm 2.11	77.08 \pm 0.72
	SAPLMA	86.87 \pm 0.73	83.89 \pm 0.28	81.15 \pm 1.84	83.06 \pm 0.87
	QAoD (V_{\perp})	87.01 \pm 0.15	82.54 \pm 0.14	79.28 \pm 0.11	79.97 \pm 0.21
	QAoD ($Q \oplus V_{\perp}$)	91.86 \pm 0.08	84.92 \pm 0.15	83.90 \pm 1.66	85.94 \pm 0.06

Table 5: Multi-seed zero-shot OOD AUROC on BioASQ (seeds 42 to 46, mean \pm std over five runs); the OOD advantage of $\mathcal{H}_{V_{\perp}}$ holds consistently across seeds.

Method	Qwen3-14B	Qwen3-30B-A3B
	BioASQ	BioASQ
MIND	47.61 \pm 2.57	64.36 \pm 2.61
SAPLMA	51.42 \pm 4.55	72.37 \pm 4.93
QAoD (V_{\perp})	77.68 \pm 0.36	76.81 \pm 0.24
QAoD ($Q \oplus V_{\perp}$)	70.52 \pm 2.15	73.93 \pm 0.76